Nordkapp TopSeis/node acquisition — Lessons from a modelling study

Jan-Erik Lie[1], Vetle Vinje[2*], Per Eivind Dhelie[1], Hao Jiang[2], Vidar Danielsen[1] and Nicolas Salaun[2].

Abstract

Based on an extensive 3D modelling study utilising full-wavefield Finite-Difference modelling and Full-Waveform Inversion (FWI) we demonstrate that the TopSeis/OBN hybrid acquisition acquired from May to August 2021 in the Nordkapp basin in the Barents Sea has the potential to image salt flanks and sedimentary details, given an accurate initial model in the shallow and a carefully designed deblending and FWI workflow. As a part of this we demonstrate that the large offsets and multi-azimuth recorded by the ocean bottom nodes are crucial to map the complex salt diapirism in the area including the steeply dipping flanks.

Introduction

The Nordkapp basin is in the south-western part of the Barents Sea and is a large, unexplored basin with proven petroleum systems containing mature Triassic source rocks (Rojo et al., 2017). Hydrocarbon exploration has mainly focused on plays defined by the salt flanks, which require a detailed knowledge of the salt geometry. However, imaging in the Nordkapp basin of the Barents Sea has been notoriously challenging due to several factors: its salt diapirism, the high seismic velocity in the sediments due to the Tertiary uplift, and a hard and irregular water bottom causing strong and complex multiples. To further complicate the imaging of the salt flanks, the acoustic impedance contrast between sediments and salt is very low which makes reflection-based imaging methods difficult.

The first wave of exploration in the area started in the 1990s and continued for about 20 years with several 2D and 3D marine surveys, electromagnetic and gravity exploration and complex model building workflows (see e.g., Hokstad et

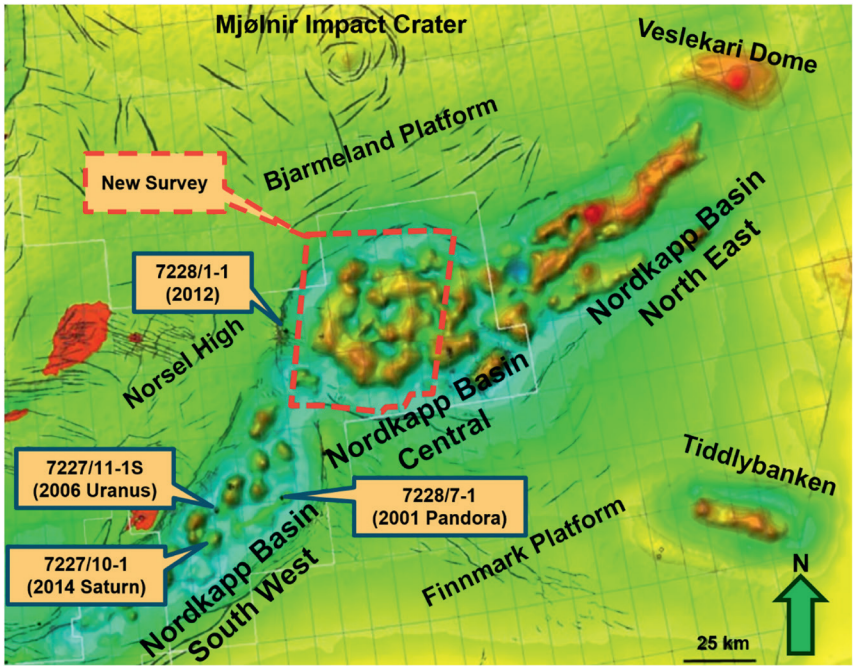

Figure 1 Map of the Nordkapp Basin showing the exploration wells, the key structural elements, and the very distinct salt diapirs. The ~3800 km^2 survey area is marked with a red dashed line.

[1] Lundin Energy Norway AS | [2] CGG
[*] Corresponding author, E-mail: vetle.vinje@cgg.com
DOI: 10.3997/1365-2397.fb2022011

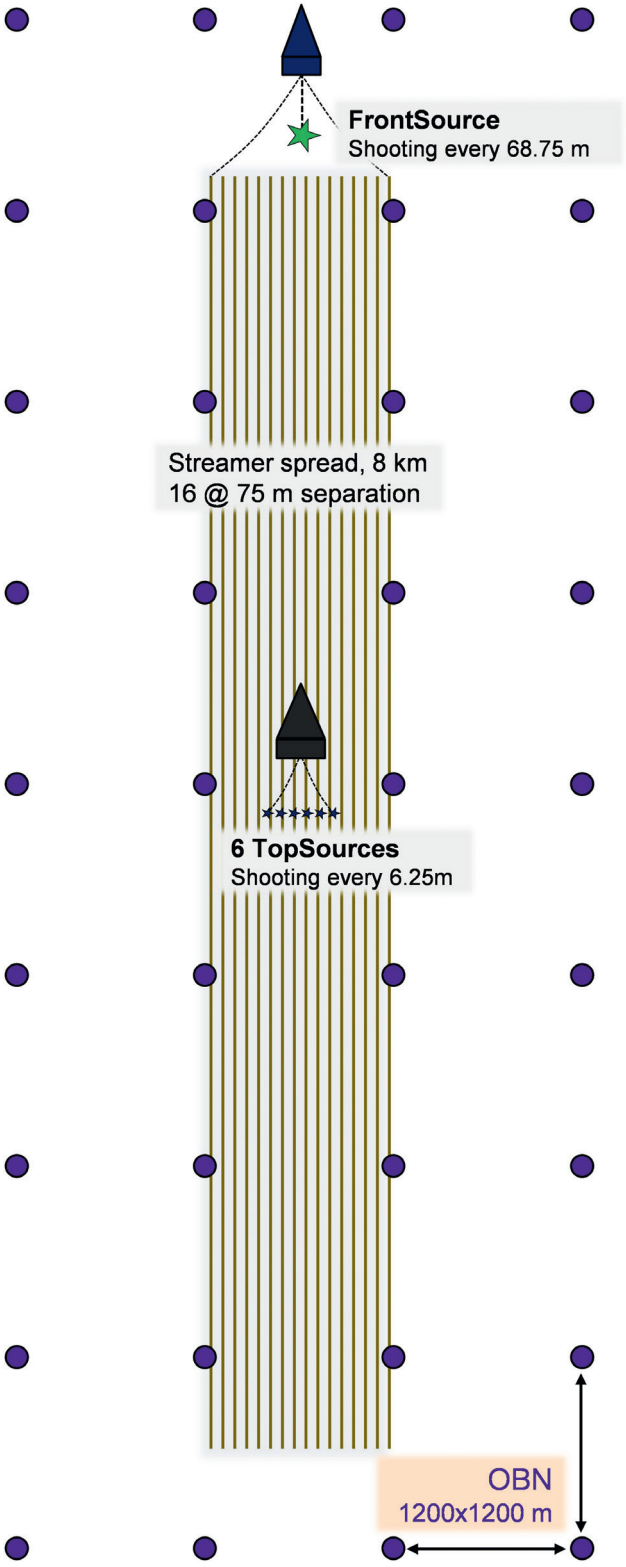

Figure 2 TopSeis/OBN hybrid acquisition with 6+1 sources and two recording systems; 16 streamers and some of the ~1000 nodes.

al. 2011 and Stadtler et al., 2014) culminating in Statoil's dry Saturn well in 2014 which was a disappointment and stalled further exploration in the area for a while. Proper mapping of the flanks of the substantial salt diapirism in the area turned out to be very difficult. The only approach that showed any promise was the coil shooting (Moldoveanu, 2008) test conducted by WesternGeco in 2013 to image the flanks of the salt walls by sailing a marine source/streamer configuration in circles around a salt dome to acquire a wide-azimuth data set. However, the coil method is not practical on a large scale and the maximum offset is limited to the streamer length. At least this approach showed the importance of wide azimuth for solving the salt-related imaging problems in the area.

Then in 2019 Lundin Energy Norway and partners were awarded the PL1083 production licence in the central Nordkapp basin shown in Figure 1 which meant that the previously mentioned persistent imaging problems were again on the table.

Part of the reason for the renewed interest in the Nordkapp basin just a few years after it was abandoned in 2014 was the prospect of finally achieving a good imaging of the complex salt diapirism through several significant improvements in both seismic acquisition and imaging technology within the last few years:

1. TopSeis, which was developed jointly by Lundin and CGG and consists in locating the sources above the streamer spread rather than in the front of it (Vinje et al. 2017). The technology was first tested in 2015 in Gabon and in the North Sea, before it was implemented in full-scale over the Loppa High in 2017 (Dhelie et al. 2018) and later over Greater Castberg in 2019 (Poole et al. 2020). TopSeis has undergone an evolution from 2, 3, 5 and 6 sources towed wider and wider making the solution more cost-effective. In addition, a large source at the front of the spread was added in the Castberg 2019 survey (Vinje, V. and Elboth, T., 2019) to obtain the long offsets required for diving wave Full-Waveform Inversion.
2. Ocean Bottom Node (OBN) acquisition has been through a renaissance with its wide-azimuth coverage and large offsets suited for imaging complex 3D bodies such as gas accumulations, injectites or salt domes.
3. FWI using diving and refracted waves to find the subsurface velocity model has been available for several years. Recently, FWI has been expanded to utilise the whole wavefield, including reflections, refractions, diving waves and multiples (Zhang et al., 2018). The resolution of FWI has increased significantly which means that the contrasts (or derivatives) in this velocity field can even be used to create an image (Zhang et al., 2020). At salt/sediment boundaries in the Nordkapp basin, there is a strong velocity gradient, which could be picked up by the velocity inversion FWI.

Already from late 2017, Lundin, in cooperation with both CGG and WesternGeco, (Branston et al. 2020) conducted evaluations and modelling studies to solve the salt-related imaging problems in the Nordkapp basin leading to the hybrid TopSeis/OBN solution described below.

We will start by describing the survey configuration which will generate four data sets, then present the risk factors, the synthetic model, the modelling approach, the deblending and finally three key experiments utilising the four datasets.

TopSeis/OBN hybrid seismic survey

On PL1083 Nordkapp, Lundin was looking for a cost- and time-effective acquisition solution which provides both shallow imaging of sediments to map the shallow upper Jurassic Real-

Name	Source	Receivers	Azimuths	Max Offsets	Primary Utility	Secondary Utility
TS	TopSource	Streamers	NAZ (except near offsets)	~4 km	Shallow imaging &VMB	HR-FWI
TSNodes	TopSource	Nodes	WAZ	Large	FWI	Deep imaging
FS	FrontSource	Streamers	NAZ	~8 km	FWI	Deep imaging
FSNodes	FrontSource	Nodes	WAZ (sparse)	Very Large	FWI (low frequency)	Deep imaging

Table 1 The TopSeis/OBN survey acquired four datasets in a single survey.

grunnen subgroup formations from the sea bottom to around 2.5 s, and reveals the deeper large-scale dome structures with their steep flanks and truncating sediments in the Triassic Snadd, Carnian and Kobbe levels. The solution was a hybrid TopSeis/OBN acquisition with six small sources (termed TopSources) deployed above 16 streamers and one single large source at the front (termed FrontSource) as shown in Figure 2.

The streamers were multi-component, and they were located at a depth of 30 m, while the nodes were dropped on the sea bottom in a coarse grid of 1200 x 1200 m to cover a large area with the ~1000 nodes available. The nodes remained on the water bottom until the end of the survey, when they were picked up by a ROV. The six TopSources were towed by a separate source vessel with 437.5 m between the outermost sources, which is wider than used on any of the other previously mentioned TopSeis surveys or any previous marine acquisition, as far as we know (Widmaier 2020). The source/streamer geometry allowed a cost-effective acquisition with as much as 600 m between the sail lines. The survey, with a surface area of ~3700 km^2 shown in Figure 1, was acquired by PGS in June-August 2021 and the complete data set was available when the nodes were retrieved and the data were unloaded by October 2021.

This unique and ambitious configuration with two source systems (TopSources and FrontSources) and two recording systems (streamers and OBNs) will, in one single survey, generate four data sets as shown in Table 1. The ambition is that the complementary nature of these four data sets will resolve the shallow and deep imaging problems mentioned above.

In Table 1 we have termed the four data sets *TS*, *TSNodes*, *FS* and *FSNodes* and listed some of the properties and potential utilities for them. The two node data sets are wide-azimuth (WAZ) with long offsets which should be an advantage for FWI, while the two streamer data sets are narrow-azimuth (NAZ) with maximum offsets limited by the streamer length, i.e., the full streamer length for FS and half the streamer length for TS since the TopSources are located in the centre of the streamer spread. The TS data should be particularly useful for shallow velocity model building (VMB) and imaging while we assume that the primary utility of the FS will be to support the FWI when used in combination with the TSNodes and FSNodes.

Note that we assume that the FSNodes data will be recorded at very large offsets since the FrontSource is significantly stronger than the TopSources with the ability to be recorded at longer distances from the sources.

A key issue in the design of this survey was the choice of a suitable separation of the TopSources, both in the x- (along the sail lines) and y- (perpendicular to the sail lines) direction. For multi-source streamer surveys, the standard approach is to spread the sources in such a way that the traces from the various sources interleave to obtain a denser bin size in the y-direction (i.e., perpendicular to the survey direction). By increasing the number of sources, we can increase the trace density in the acquisition. The bin size in the y-direction is given by DS/(2*NS), where DS is the streamer separation and NS is the number of sources. There has been a trend towards more sources, for instance increasing from two sources to three as suggested by Langhammer and Bennion in 2015, or even up to five as deployed in the TopSeis Castberg survey, (Poole et al. 2020) or six sources as in the 2021 TopSeis/OBN survey that we discuss in this paper. In order to optimise the shallow imaging, we decided to both spread the TopSources as far out as possible, as well as using the interleaving principle with 87.5 m y-separation between the sources giving a bin size of dy=75/(2*6)=6.25m. The bin size in the x-direction is half the receiver separation, i.e., dx=12.5/2= 6.25 m. For the FS data (i.e., the single FrontSource shooting into the streamers) the bin size is (dx, dy) = (6.25 x 37.5) m. In Figure 3 the irregular shot carpet is displayed for three sail lines going south-north with 600 m between the FrontSources (which is the sail line separation), 87.5 m between the six TopSources in a sail line and 162.5 m between the outermost TopSources on adjacent sail lines. The sources were not spread in a regular shot carpet because we needed large sail line separation to ensure cost efficiency and there are equipment limits on how wide it is possible to tow the sources.

Any seismic data is defined in a four-dimensional space of traces consisting in spatial location of their CMP (x,y) and their offset vector (x-offset, y-offset). The offset vector (x-offset, y-offset) is the vector in the xy-plane pointing from the source to

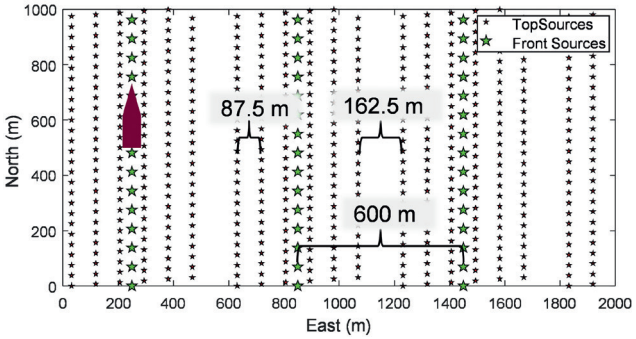

Figure 3 Source point distribution in the TopSeis/OBN survey for three sail lines going from south to north shown in true aspect ratio.

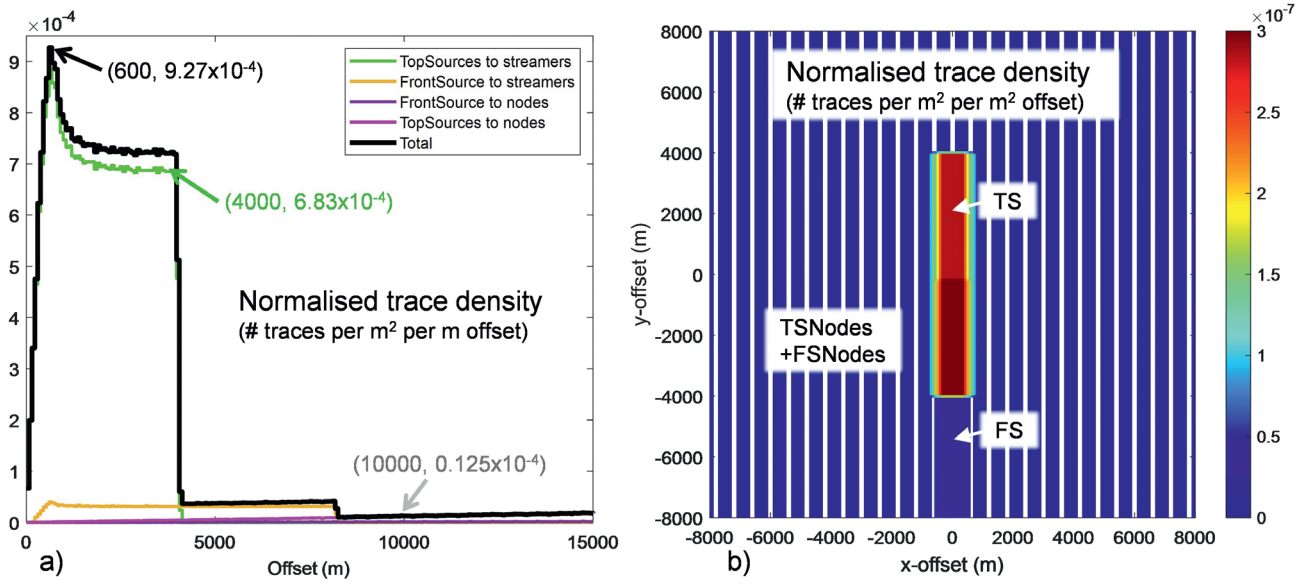

Figure 4 Normalized trace density as a function of a) absolute offset and b) offset vector (x-offset, y-offset).

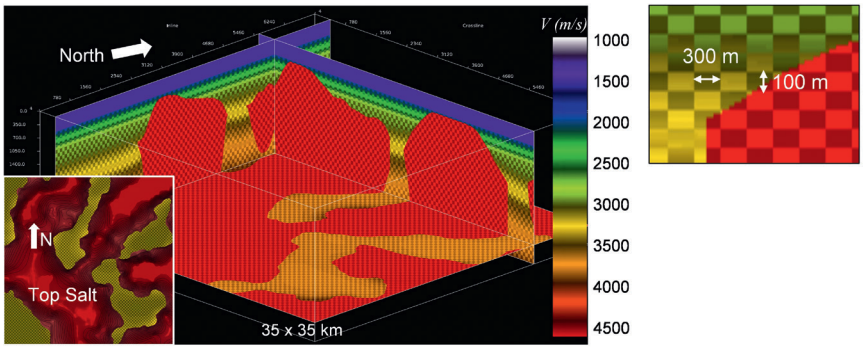

Figure 5 The true model in which the synthetic seismic is modelled by Finite Difference modelling. A checkerboard pattern with velocity variations between (-50 to 50 m/s) is included.

the receiver. Figure 4a displays the normalised trace density per absolute offset and Figure 4b as a function of the offset vector. The absolute offset (simply called 'offset' below) is the horizontal distance between the source and receiver, i.e., the length of the offset vector. The four data sets in Table 1 have different bin sizes and different offset class sizes, so to facilitate a quantitative comparison of the trace density between them, the trace density values were normalised, not only with respect to the xy, but also with respect to offset. For instance, in Figure 4a the trace density is the number of traces per square metre in the xy-plane and for each metre offset. If we want to know the trace density for a (6.25*6.25) m bin cell and for an offset class size of 75 m which correspond to the native bin/offset of the TS data, we multiply the trace density with 6.25*6.25 *75. If we then consider the TS curve in Figure 4a at 4000 m offset (green arrow) the trace density is 6.83×10^{-4} traces per m^2 per m offset which correspond to 6.83×10^{-4} * 6.25*6.25 *75 = 2 traces per (6.25 x 6.25) m bin and 75 m offset class, which is exactly as expected for the split-spread TopSeis data.

From Figure 4a, we also notice the very high trace density of the TS data which drops to zero at 4000 m offset. At this point, the FS data becomes dominant, and the trace density remains flat until it runs out of streamer offsets at 8200 m. After that point, we only rely on the node data, which displays a linear increase with offset but with a significantly lower trace density than the streamer data. At 10,000 m offset (grey arrow in Figure 4a) the total trace density is only about 1.3% of the trace density at the peak at 600 m (black arrow).

Figure 4b shows the normalised (# traces per m^2 pr m^2 offset) trace density in the offset vector plane. These plots are termed rose plots, but they are usually not displayed in normalised form. The plot goes from -8000 to 8000 m x-offset and y-offset, and the imprint of the high-density but narrow-azimuth TS with maximum 4000 m offset is clearly visible. The imprint of the FS stretches towards south all the way down to 8000 m offset, while the two node surveys cover the entire xy-offset plane with an approximately constant but very low trace density. The gap of 162.5 m between the outermost sources on neighbouring sail lines manifests itself as the thin vertical white lines with no illumination.

Risk factors and motivation behind this modelling study

However, there are a few risk factors here:

(i) The top sources fire every ~2.5 s and the large front source every ~27.5 s, so there will be a severe blending of data, especially on the long offsets required for the large-scale imaging of the salt diapirs.

(ii) The node data are sampled sparsely. For water depths of 300-400 m, as present on the Nordkapp basin, node samplings

between 25-400 m have been the norm in the North Sea (Thompson et al., 2002). In the Nordkapp case, the node separation is 3-48 times larger. This is obviously too coarse for conventional imaging, but is it sufficient for FWI.

(iii) Conventionally, when shooting an OBN/OBC survey, a uniform shot carpet of 50x25 m sampling (i.e., 800 shots per km^2) is the norm (Thompson et al., 2002). In the Nordkapp TopSeis/OBN hybrid project, there are 6+1 sources in the survey giving a shot-point distribution as shown in Figure 3 with 87.5 m between the TopSources and gaps between the outermost sources of neighbouring sail lines of 162.5 m. The shot density will be only 291 shots per km^2. Will this source configuration be adequate for the node data sets in Table 1?

The primary purpose of this modelling study is to investigate and quantify the effect of these three risk factors, and to what extent we will be able to use the long offsets and all-azimuths illumination of the node data to resolve the imaging problems. The focus will be to investigate the ability of FWI (Zhang et al., 2018) to map the deeper salt flank-related targets below ~1 s by utilising a combination of the four data sets in Table 1.

Furthermore, we will investigate the importance of the accuracy of the *Initial Model*, i.e., the starting model going into the FWI.

The aim of the modelling study is to demonstrate the potential of the used survey design and not to optimize it. This could be addressed with a series of comparative modelling studies which is beyond the scope of the current study.

The Nordkapp velocity/density model

This study is based on 3D acoustic Finite-Difference modelling of all the four data sets in Table 1 for which we need a 3D velocity and density model. A 35x35 km central part of the survey area over PL1083 is chosen. Sixty-four previously acquired and processed 2D lines were interpreted to create a map of the top salt. The salt diapirism is extensive, with salt bodies in the shape of ridges and domes partly going all the way up to the water bottom. The imaging of the salt flanks was poor on the 2D lines. Thus, both creative imagination and information about the sedimentation and geological history were used to create realistic salt walls. In-between the salt, there are relatively narrow basins of sedimentary layers where we used a combination of the few wells in the Nordkapp basin and available seismic information to create the isotropic velocity model. In the sediments we used the Gardner's formula for the density ($r=0.31 \cdot V^{0.25}$), while in the salt we used a typical salt density of 2.2 g/cm^3.

In our study, we term this model the *True Model*. In Figure 5, the velocity model with the top salt interpretation is presented. As can be seen in this figure, we also inserted a 3D rectangular checkerboard perturbation onto the velocity beneath the water bottom. The magnitude of this perturbation is from -50 to 50 m/s. This artificial feature represents the detailed, small-scale variations

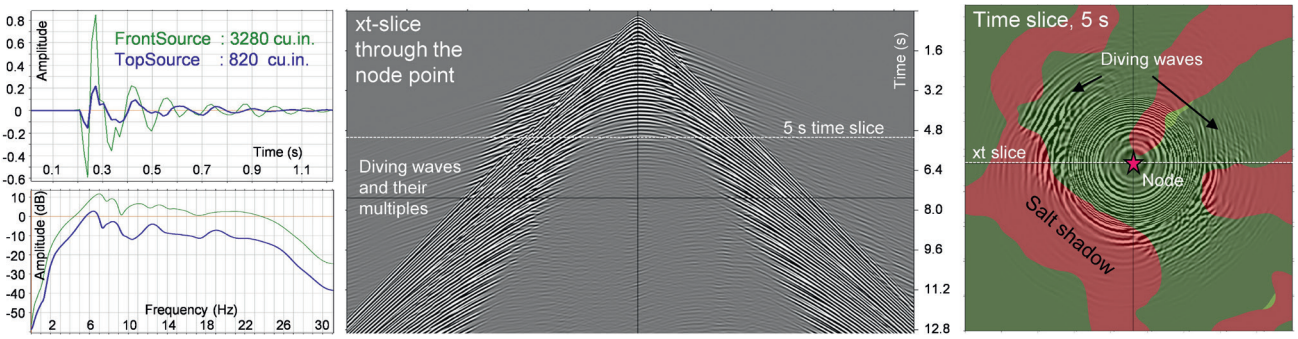

Figure 6 Source signature of the FrontSource and TopSource used in the modelling a) and an example of a node gather from the modelling with an xt-slice in b). In c) we display a time slice at 5 s through the node gather overlain by a depth slice through the True Model showing the location of the salt (red) and sediments (green) at a depth of 750 m.

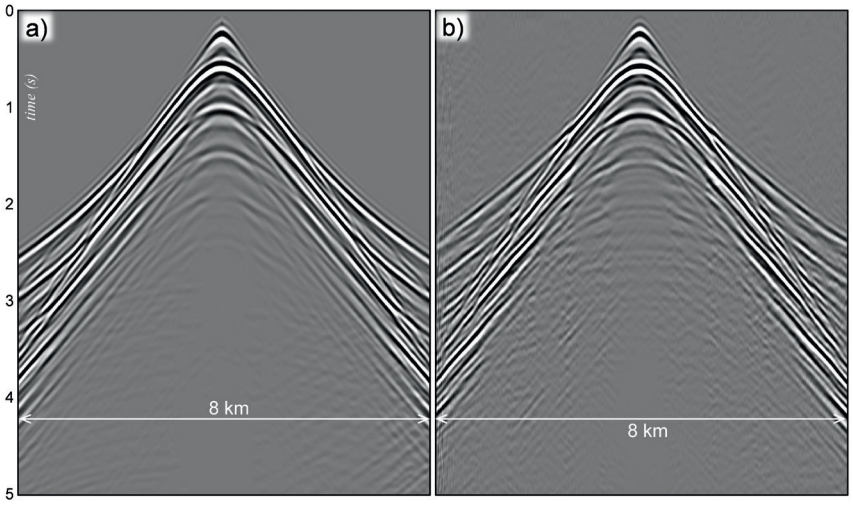

Figure 7 Modelled a) and deblended real b) shot gather from a TopSource to a streamer.

of velocity in the real model which are found in the sedimentary layering and faulting as well as in intrusions in the salt bodies.

The Finite Difference modelling

In the True Model, we simulate all the four data sets in Table 1 using acoustic Finite-Difference modelling with the source signatures from the TopSeis Castberg survey (Poole et al. 2020). The computation of thousands of synthetic shot gathers in 3D is quite expensive, so we limit the bandwidth to 20 Hz in the modelling. The FrontSource is about four times larger in volume and amplitude than the TopSources. Figure 6a shows the two source signatures with spectra, while 6b and 6c show a node gather in the centre of the model, where we can clearly see the shadow effect of the salt in the diving waves on both the xt-slice (b) and time slice (c). Furthermore, we can observe the diving waves and their free surface multiples arriving first on the far offsets, the strong guided wave train in the water column and the weaker primary and multiple scattering from the water bottom, the salt boundary, and the checkerboard pattern.

At the time of writing, we received the first real shot gathers recorded in the streamers from the PGS acquisition. In Figure 7, an unblended modelled TS shot gather (a) is compared with a deblended real shot gather from the field (b), both lowpass filtered at 15 Hz. There is a striking similarity between them, which is good news for the accuracy of this modelling study.

Blending and deblending

The six TopSources provide a shot carpet as shown in Figure 3, which makes them suitable for both shallow imaging using the streamers and as sources for the sparse node layout. However, such a dense shooting from one single source vessel will also create significant blending. In addition, the FrontSource will also contribute to the blending problem. In Figure 8, the blended data is shown in a streamer (a) and for a node gather (b). In the streamer, a single Front Source and five consecutive TopSources, firing every ~2.5 s, are visible within the ~12 s record shown here. To limit the blending, the Front Source shoots only every 11th TopSource, i.e., at ~27.5 s. A random dither is added to the shooting.

In Figure 8b, we show a node gather (i.e., the traces corresponding to a line of TopSources shooting into a single node along an inline). The crosstalk/blending in this gather is very strong and appears as a random burst of noise. Deblending this data to provide clean versions of the four data sets in Table 1 is challenging.

The deblending was performed by a complex workflow centred around an inversion algorithm combining sparse tau-p transforms and HARCWT inversion (Peng and Meng, 2016). This gave estimates of the de-blended residues and of the different orders of blending pollutions (i.e., from the previous shot and second next shot-point). In the following section, we will term these data the *deblended* datasets. The record length of these is 12 seconds. The tests to follow below will include both deblended as well as *unblended* data sets. Examples of such an unblended (i.e., clean) data set are shown in Figure 6b and Figure 7a.

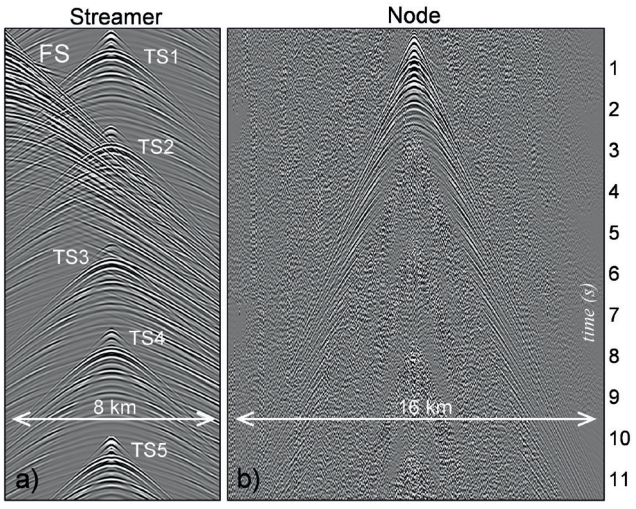

Figure 8 Blended datasets as expressed in a streamer and in a node.

The initial model

It is well known that the success of FWI depends on an accurate initial velocity model. In the Nordkapp case, the streamer data will be available before the node data, which means that the densely sampled streamer data from the TopSources, rich in near-offsets, can be used to build a fast-track shallow velocity model of the sediments down to the top salt, which can also be picked. The flanks of the salt, however, will most probably not be visible on the fast-track processing; consequently, the best we can do in the initial model is to assume vertical flanks starting from the edges of the salt.

We will test three versions of the initial model: **IMOD_A** with no error in the shallow sediment velocity, **IMOD_B** with 5% underestimation of the velocity and **IMOD_C** with 20% underestimation of the velocity. In all the models:

1. the vertical two-way traveltime to the top salt is preserved
2. The top salt is flooded vertically starting from the edge of the salt
3. The velocity is smoothed, mild in the shallow and more in the deep.
4. No checkerboard pattern is present

A small part of the three initial models and the true model are shown in Figure 9. Notice that the smoothed top salt in initial models B and C is located too shallow due to the underestimation of the sediment velocities, particularly for IMOD_C (white

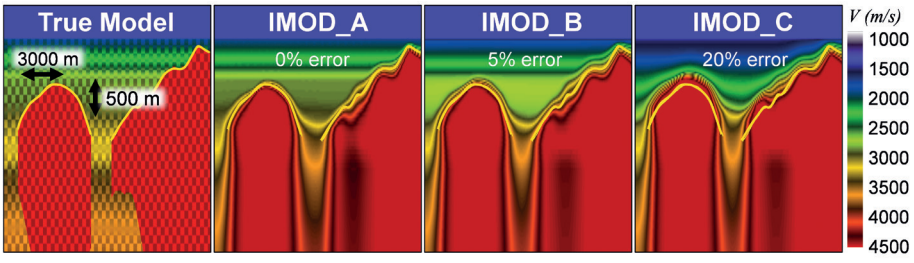

Figure 9 A select portion of the true model and the three initial models with decreasing level of inaccuracy in the sediment velocity. The true top salt is shown as a thick, yellow line.

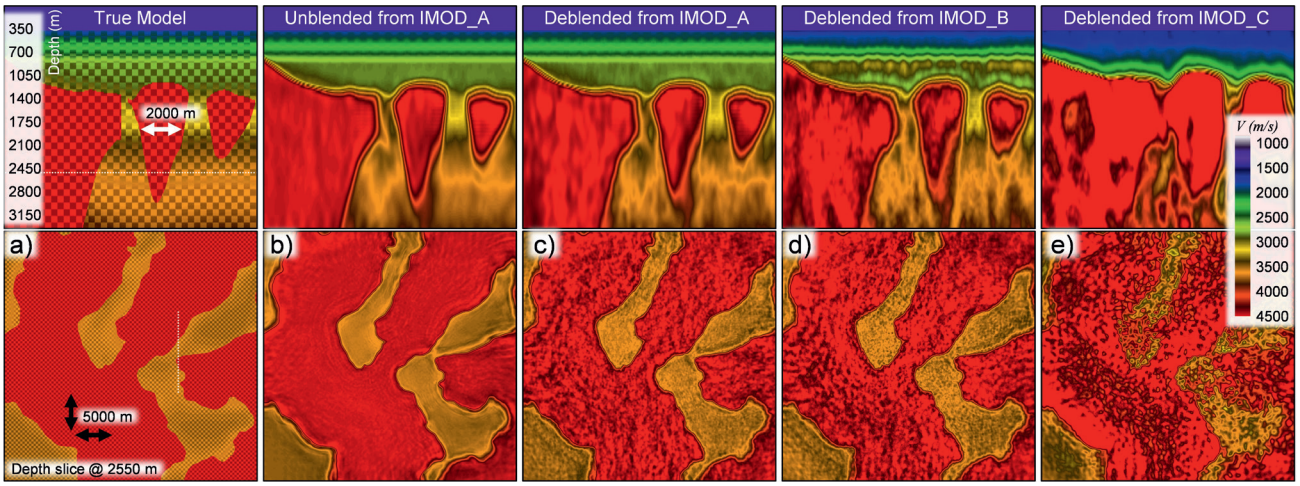

Figure 10 Inversion results for the Top Source Node data for unblended and deblended data and for the three initial models. The error in the shallow sediment velocity in IMOD_C (20%) is too large to avoid cycle skipping and the FWI result is poor.

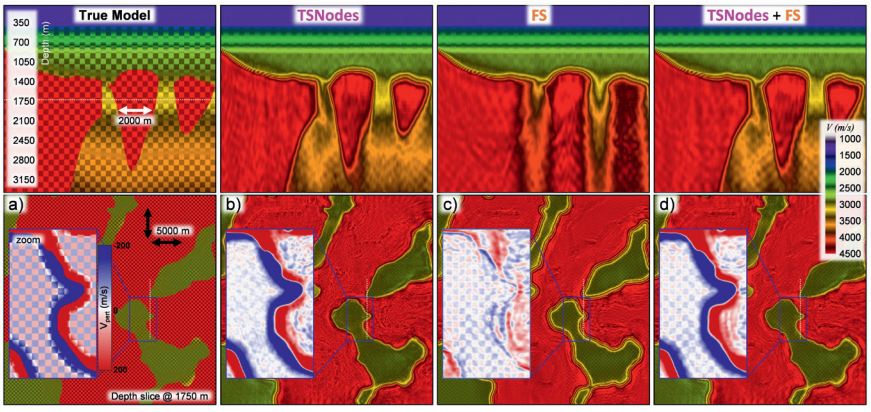

Figure 11 FWI results for (b) unblended TSNodes data, (c) FrontSource to streamer data and (d) both data sets. The first column, (a), is the true model.

arrow). For all the initial models, we use the same constant density model of 1.645 g/cm^3 below the water bottom.

First experiment: the effect of blending and the accuracy of the initial model

We start by investigating the effect on the FWI of (i) using unblended vs deblended data and (ii) the accuracy of the initial model. For this we use TSNodes, the data from the TopSources recorded in the nodes. All the FWI tests used the same number of iterations and were done successively from 2.7 to 10 Hz. The maximum source-receiver offset is 15 km.

Figure 10 shows a central inline and a depth slice at 2550 m through the velocity model for (a) the true model, (b) the FWI result using unblended data and the initial model IMOD_A, while (c), (d) and (e) are FWI using deblended data and initial model IMOD_A, IMOD_B and IMOD_C respectively. The location of the inline and depth slice is indicated by the dotted white lines in the True model in column a).

As expected, we see a significant increase in noise from columns (b) to (c) due to the crosstalk introduced by the blending, but in both cases the salt definition is good, even in the salt overhangs. Also, when using a slightly more inaccurate initial model in column (d) the salt definition is good. However, when using IMOD_C with 20% error in the sediment velocity FWI does not converge and the result is unacceptable.

There is not much sign of the checkerboard pattern, except for some faint hints just below the water bottom in columns (b) and (c).

As mentioned above, we used 15 km maximum offset in all the TopSource to Nodes data tests in Figure 10 and demonstrated a good salt definition even for deblended data and up to 5% error in the starting model. We have also tested maximum offset of 8 km, which is too short to reveal the true salt model, especially in the deep.

Second experiment: using TSNodes and FS jointly

We noticed in Figure 10 above that the checkerboard pattern in the True model was still invisible in the updated models using the TSNodes data alone up to 10 Hz. This may not be surprising as this data set is very sparse, with 1200 m between the nodes and up to 162.5 m between shot points in-between the sail lines as shown in Figure 3. We now proceed by including the FS data (i.e., the energy from the FrontSources recorded in the streamers) and combine it with the TSNodes data. For all the tests, we use IMOD_A as the initial model and unblended data.

The results are displayed in Figure 11 with each column being a central inline (top) and a depth slice at 1750 m (bottom) of (a) the true model, (b) FWI using TSNodes data alone, (c) FWI using FS (FrontSource to streamers) data alone, and finally, (d) combining TSNodes and FS data. In the depth slices, the zoom shows the perturbation from the initial model plotted with

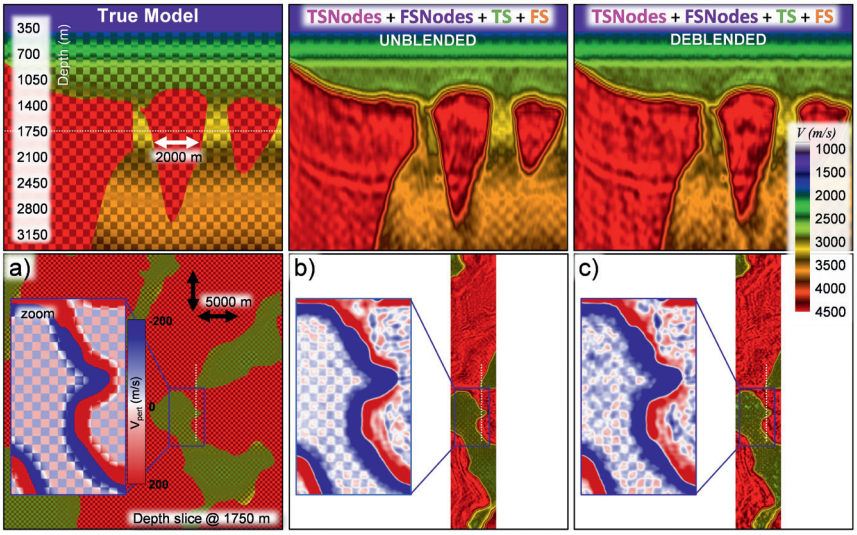

Figure 12 FWI results for all four data sets for b) unblended and c) deblended data. In both tests we used an initial model with 5% error in the sediment velocity. The first column, a) is the true model.

a separate colour scale from -200 to 200 m/s. For column (a), this is the difference between the True model and IMOD_A. For column (b), (c), and (d), it is the velocity perturbation from the True Model to the FWI results.

To make the FWI results comparable we run the same number of iterations for both (b), (c), and (d) using the following strategy:

TSNodes data only, column (b)

from 2.7 to 10 Hz with max offset 15 km

from 10 to 15 Hz with max offset 8 km

FS data only, column (c), using the maximum recorded offset of 8 km

from 2.7 to 10 Hz with max offset 8 km

from 10 to 15 Hz with max offset 8 km

TSNodes + FS data, column (d)

TSNodes: from 2.7 to 10 Hz with max offset 15 km

FS data: from 10 to 15 Hz with max offset 8 km

Figure 11 shows that the TSNodes data with its long offsets and wide azimuths is needed to find the salt boundaries, while the narrow-azimuth, but dense, FS data is required to reveal the checkerboard. The zoom in the depth slices shows the difference between the initial model and the FWI results. When both data sets (TSNodes and FS) were used, as shown in column (d), we achieve both salt definition as well as resolution of the checkerboard pattern in the sediments. This illustrates the complementary properties of these two data sets when used in FWI.

Third experiment: realistic initial model, effect of deblending and using all data

In the final, and most realistic experiment in this paper, we will use all four data sets in Table 1 and the 5% inaccurate initial model IMOD_B. We use IMOD_B in this test because it is a reasonable approximation of the initial model that will be used in the FWI from the real TopSeis/OBN data from the Nordkapp Basin. In the real processing, we will use the streamer data and conventional velocity model-building techniques (RMO picking & tomography) to obtain a reasonable (but not 100% accurate) estimation of the shallow sediment velocities above the first water bottom multiple. Furthermore, we assume that it will be possible to pick the top salt on the streamer data. Finally, given no salt flanks will probably be visible at this stage, we will flood vertically with salt velocity.

Figure 12 shows the result of this experiment with column (a) the true velocity, (b) the FWI using unblended data, and (c) FWI using deblended data. Only five sail lines of the streamer data (FS and TS) were used in the FWI to limit the large computational costs for modelling, deblending, and FWI. The FWI models in columns (b) and (c) are therefore only shown for the 3 km-wide north-to-south strip covered by these five sail lines. However, the FWI results within this strip are equivalent to what would have been achieved if all the sail lines in TS and FS were included.

The FWI for both (b) unblended and (c) deblended data has been performed using the following strategy where the output velocity from one step is fed into the next step:

TSNodes: from 2.7 to 6 Hz with max offset 15 km

FSNodes: from 2.7 to 6 Hz with max offset 15 km

TSNodes: from 6 to 10 Hz with max offset 15 km

FSNodes: from 6 to 10 Hz with max offset 15 km

FS and TS alternating: from 10 to 15 Hz with max offset 4 km (TS) and 8 km (FS)

When using the unblended data as input to FWI as shown in Figure 12b, the salt and the checkerboard pattern are better defined than in Figure 11d where only TSNodes and FS were used. When we use deblended data as input to FWI as shown in Figure 12c, the salt boundaries are still well defined, but the checkerboard resolution is poorer.

Concluding remarks

Any modelling study will apply a set of simplifications to real-world phenomena. These simplifications are required due to our limited knowledge of the physical reality and the limitations in compute resources. In this modelling study, we use isotropic models with acoustic wave propagation and no anelastic attenuation of the propagating waves. Furthermore, we do not include ambient noise. However, we do consider the reflections from the sea surface (multiples), real source signatures, blending

of the data caused by the dense shooting and the idealised 3D geometry of sources and receivers in this unique TopSeis/OBN survey. We also use state-of-the art deblending tools and the latest FWI (Zhang et al., 2018), which will also be used for the real data from the Nordkapp basin.

The findings from this modelling study can be summarised as:

- The streamer data (FS and TS) reveal details in the sediments, but are not able to image the deeper flanks of the complex salt bodies
- The node data (TSNodes and FSNodes) give an excellent definition of the salt model despite their low trace density. However, they are almost blind to the checkerboard details in the sediments with the max 15 Hz used in this study
- Combining node data and streamer data gives both good salt as well as sediment definition
- The blending does not harm the salt definition but introduces a significant amount of noise into the sediment inversion results
- FWI starting from 2.7 Hz tolerates an initial model with 5% error in the shallow sediments, but breaks down if the error is 20%

Thus, from this modelling study, we conclude that complementary geometrical properties of the streamer and node data in this TopSeis/OBN survey provide both good salt definition as well as details in the sediments, which was Lundin's intention with this unique set-up. However, the final answer regarding the level of success of this survey will come later, when the real Nordkapp TopSeis/OBN data is available and is processed through a complete processing, imaging and FWI workflow with higher frequencies than the 15 Hz tested in this study.

Acknowledgements

We would like to thank Sylvain Masclet, Guillaume Henin, Isabel Espin and Andrea Roubaud in CGG's Massy processing centre for the deblending of the data and their support in the modelling and FWI. We also thank Steve Thompson and Peng Zhao from CGG's Crawley and Oslo centres, respectively, for the model building.

References

Branston, M., Aarnes, A., Raknes, E., Nilsen, E., Campbell, R., Barlass, D., Apeland, G., Jørgensen, J. and Lie, J.E. [2020]. Designing an Acquisition Solution for the Nordkapp Basin, Second EAGE Marine Acquisition Workshop, Extended Abstracts.

Dhelie, P.E., Danielsen, V., Lie, J.E., Kjelsrud Evensen, A., Wright, A., Salaun, N., Rivault, J.L., Siliqi, R., Grubb, C., Vinje, V. and Camerer, A. [2018]. Improving seismic imaging in the Barents Sea by source-over-cable acquisition, 88th SEG annual Meeting, Extended Abstracts.

Hokstad, K., Fotland, B., Mackenzie, G., Antonsdottir, V., Foss, S.K., Stadtler, C., Fichler, C., Haverl, M., Traub Waagan, M., Myrlund, E.A., Masnaghetti, L., Ceci, F. and Raya P.Y. [2011]. Joint imaging of geophysical data: Case history from the Nordkapp Basin, Barents Sea. 81st SEG annual Meeting, Extended Abstracts.

Langhammer, J. and Bennion, P. [2015]. Triple-Source Simultaneous Shooting, A future for higher density seismic. 77th EAGE Conference & Exhibition, Extended Abstracts.

Moldoveanu, N. [2008]. Circular geometry for wide-azimuth towed-streamer surveys. 70th EAGE Conference and Exhibition, Extended Abstracts, 55-59.

Peng, C. and Meng, J. [2016]. Inversion-based 3D deblending of towed-streamer simultaneous source data using sparse TauP and wavelet transforms. 86th Annual International Meeting, SEG, Expanded Abstracts.

Poole, G., Cichy, K., Kaszycka, E., Vinje, V. and Salaun, N. [2020]. On Top of Seismic Sampling – Benefits of High-Resolution Source-Over-Streamer Acquisition. 79th EAGE Conference & Exhibition, Extended Abstracts.

Rojo Moraleda, M. L., Cardozo, N. and Escalona, A. [2017]. Controls on suprasalt deformation in the Nordkapp Basin, Norwegian Barents Sea. 77th EAGE Conference & Exhibition, Extended Abstracts.

Stadtler, C., Fichler, C. Hokstad, K., Myrlund, E., A., Wienecke, S., and Fotland, B. [2014]. Improved salt imaging in a basin context by high resolution potential field data: Nordkapp Basin, Barents Sea. *Geophysical Prospecting*, 62, 615-630.

Thompson, M., Amundsen, L. and Duffaut, K. [2002]. Acquisition geometry versus 4C image quality – a study of Statfjord, and Gullfaks Sør. 64th EAGE Conference & Exhibition, Extended Abstracts.

Vinje, V., Lie, J.E., Danielsen, V., Dhelie, E., Siliqi, R., Nilsen, C-I., Hicks, E. and Camerer, A. [2017]. Shooting over the streamer spread. *First Break*, **35**(6), 97-104.

Vinje, V. and Elboth, T. [2019]. Hunting high and low in marine seismic acquisition; combining wide-tow top sources with front sources. 78th EAGE Conference & Exhibition, Extended Abstracts.

Widmaier, M., Tønnesen, R., Oukili, J. and Roalkvam, C., [2020] Recent advances with wide-tow multi-sources in marine seismic streamer acquisition and imaging. *First Break*, **38**(12), 75-79.

Zhang, Z., Mei, J., Lin, F., Huang, R. and Wang, P. [2018]. Correcting for salt misinterpretation with full-waveform inversion. 88th SEG Annual International Meeting, Expanded Abstracts, 1143-1147.

Zhang, Z., Wu, Z., Wei, Z., Mei, J., Huang, R. and Wang, P. [2020]. FWI Imaging: Full-wavefield imaging through full-waveform inversion. 90th SEG Annual International Meeting, Expanded Abstracts, 656-660.